Excitation of a Parallel-Plate Dielectric Waveguide Using a Coaxial Probe—Basic Characteristics and Experiments

Godfrey K. C. Kwan, *Member, IEEE,* and Nirod K. Das, *Member, IEEE*

***Abstract*—In this paper, we study the basic characteristics of a probe excitation to a parallel-plate dielectric waveguide (PPDW), and present design data and experimental results. A coaxial probe has been used in microstrip lines and rectangular waveguides. The present study shows that it is also an effective method to excite/couple a PPDW, thus facilitating the introduction of a new class of PPDW technology in microwave/millimeter-wave integrated circuits. We use here a spectral-domain analysis for analytical modeling of the probe transition, where the probe is approximated by a current strip of an equivalent width. Applying the method of image, the structure is transformed to an infinite-long thin strip inside a dielectric slab, which reduces the transition analysis into a simpler planar geometry. Basic characteristics of the probe excitation, and a complete design data for the radiation loss, excitation efficiency, and input impedance for various transition parameters are computed. Prototype design experiments were conducted, which show that quite efficient excitation can be achieved using the probe, with insertion loss as low as 0.1 dB. This is contrary to some misconceptions that a probe transition to the fundamental PPDW mode is quite inefficient due to parallel-plate mode radiation.**

***Index Terms*—Coaxial to dielectric waveguide transition, coaxial transition, dielectric waveguide, nonradiative dielectric waveguide.**

I. Introduction

MULTILAYER microwave and millimeter-wave integrated circuits/antennas are attractive for high-density integration in multiple levels [1], [2]. In such applications, the independent circuit layers need to be electrically isolated from each other by metal planes, resulting in stacked parallel-plate structures. The printed-circuit technology may be used for the integration, with stripline as the transmission line of choice (some form of conductor-backed slotline or coplanar waveguide may also be used), and with via-holes or slots as mechanism of signal transfer between layers. However, this will create the problem of excitation of the parallel-plate modes at various junctions. The level of parallel-plate-mode excitation can often be prohibitively large, leading to power loss and/or unwanted crosstalk between components. Besides radiation from the junctions, under nonideal conditions of having air gaps or bonding films between layers (left during fabrication process), the stripline may excite distributed radiation to leaky modes [3], [4]. Use of shorting pins may alleviate the above problems by providing short-circuiting paths between the metal planes. However, that may mean drilling too many shorting posts all over the circuit [5], which is practically undesirable. Similarly, a "dielectric plug" fabricated around a slot-type transition may help to confine/minimize the parallel-plate radiation, with only limited benefits [6].

We propose the use of a parallel-plate dielectric waveguide (PPDW) as a preferred guiding medium inside the parallel-plate layers. As the name suggests, the PPDW consists of a rectangular dielectric strip embedded between two parallel metallic plates (see Fig. 1). Unlike a stripline, the PPDW is a dielectric-guide structure that cannot be "printed," but can be fabricated with relative ease using automated machining process for

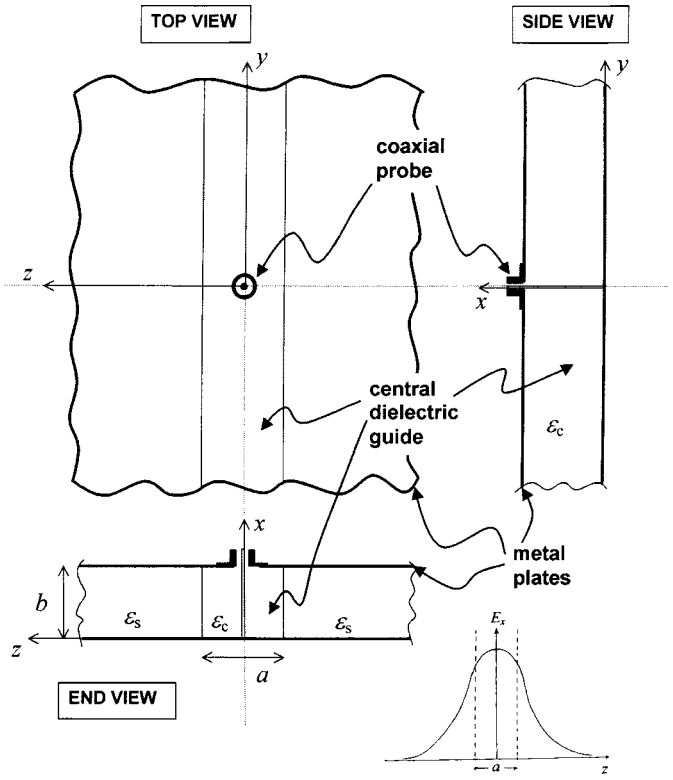

Fig. 1. Geometry of a coaxial to PPDW transition. a = width of the center dielectric strip, b = thickness of the substrate, ϵ_c = dielectric constant of the center dielectric strip, ϵ_s = dielectric constant of the outside dielectric substrate.

Manuscript received January 18, 1999; revised January 4, 2001. This work was supported in part by the Army Research Office under Grant DAAH04-95-1-0254.

G. K. C. Kwan was with the Weber Research Institute/Department of Electrical Engineering, Polytechnic University, Farmingdale, NY 11735 USA. He is now with Agilent Technologies, Rohnert Park, CA 94928 USA.

N. K. Das is with the Weber Research Institute/Department of Electrical Engineering, Polytechnic University, Farmingdale, NY 11735 USA (e-mail: ndas@photon.poly.edu).

Publisher Item Identifier S 0018-9480(02)05211-0.

lower microwave frequencies. It may also be fabricated using a microelectronic deposition process for higher frequency applications in order to achieve much better dimensional accuracy. The problems due to the parallel-plate-mode excitations, as discussed above, can be potentially eliminated or minimized by use of the PPDW. The guiding mode of a PPDW is the fundamental TE_{10} mode, which supports an electric field (equivalently, a voltage) across the parallel plates. The PPDW mode is a nonradiating mode, in the sense that its fields are confined or bound to the central guiding region. Therefore, it does not suffer from the leakage problem experienced by a stripline. Further, if a PPDW will be used in place of a stripline, any parallel-plate radiation from a coaxial probe or a slot (needed for transition across a metal plane) will be confined and guided by the surrounding PPDW structure due to total reflection from its outer dielectric interfaces. This is in distinct contrast to a stripline structure, where any voltage applied or dynamically induced across the parallel plates cannot be confined locally, but turns into the unwanted parallel-plate radiation. In addition to the above strategic advantages of a PPDW, it is also a lower loss waveguiding medium compared to a printed line. Printed lines are usually lossy at higher frequencies due to high currents at the sharp edges of the metal strips. In contrast, the PPDW does not use any metal edges for guidance, with most of the signal power confined in the dielectric medium, leading to the reduction in the loss.

It may be mentioned that the physical structure of the PPDW is similar to an H-guide, or a noradiative dielectric (NRD)-guide [7]–[9]. However, both the H- and the NRD-guides chose to use higher order modes of the structure for their operation. These higher order modes have cutoff behavior, and would require thick parallel-plate separation for operation, particularly for lower frequency applications. In addition, multimodal behavior of the NRD- and H-guides lead to complexity in layer-to-layer transition designs and mode-suppression arrangements. In contrast, the PPDW uses the fundamental TE_{10} mode, which operates down to dc, allowing the use of thin waveguides for a range of microwave and millimeter-wave frequencies. The single-moded operation of the PPDW will also allow the design of simple transitions (as presented in this paper) without the multimodal excitation problems faced by the NRD- and H-guides.

Design of suitable methods of excitation/coupling is the first step to future applications of the PPDW. In this paper, we will present the theoretical and experimental investigation of a coaxial excitation to a PPDW. Coaxial transitions have been successfully used to excite microstrip structures [10]–[13] and rectangular waveguides [14]–[19]. Here, we will show that the coaxial transition can be successfully used to excite a PPDW from across one of its ground planes, as shown in Fig. 1. The principle can be extended to multiple layers, with the probe connecting to PPDWs across isolation metal planes [20], [21]. This will facilitate the use of the PPDW in multilayer microwave/millimeter-wave circuits. We will first briefly discuss the propagation and modal characteristics of the PPDW itself, as relevant to the modeling and design of the coaxial-to-PPDW transition. A spectral-domain analysis will then be used to model the coaxial-to-PPDW junction, where the probe is approximated by a metal strip of an equivalent width. Via imaging across the parallel plates, the strip is transformed into a simpler planar geometry having an infinitely long current strip inside a dielectric slab of infinite lateral extent. Various basic characteristics and design data for the radiation efficiency and input impedance of the probe are computed for a range of physical parameters of the PPDW and probe. Based on the theoretical analysis, an accurate circuit model is also derived that can be used to simplify the design process. Prototype two-port circuits consisting of a PPDW, coupled at the two ends by PPDW-to-coaxial transitions, are designed and tested. The experimental results validate the theoretical data and demonstrate the practicality of the transition.

First, Section II briefly discusses the characteristics of the PPDW itself, followed by the analysis and circuit modeling of the coax-to-PPDW transition presented in Section III. Computed data for the transition and experimental results for a prototype design are presented in Section IV.

II. PPDW Characteristics

The geometry of the PPDW, together with the excitation using a coaxial probe at the center, is shown in Fig. 1. a is the width of the central dielectric strip and b is its height. As discussed, our focus here is on the fundamental TE_{10} mode in the waveguide, the profile of the x-directed electric field for which is also shown alongside Fig. 1. In order to be compatible with the coordinates used in the analysis of Section III, in Fig. 1, we have used $\hat{y}$ as the direction of propagation, and the x–z-plane as the cross-sectional plane of the PPDW guide. The dielectric constant of the central guide is equal to ϵ_c, and that of the surrounding medium ϵ_s, with $\epsilon_c > \epsilon_s$. ϵ_s, in general, can take any value less than ϵ_c.

Following a standard practice, all the guided modes in the PPDW structure can be classified into two complementary mode sets, i.e., the TE_z, transverse electric to the z-direction, and the TM_z, transverse magnetic to the z-direction. Solving for the Maxwell's equations, separately for the TE_z and TM_z modes, with proper boundary conditions [22], the dispersion behaviors of various modes can be derived. Dispersion relation for the fundamental TE_{10} mode (the PPDW mode), which can be shown to be the same as that for an infinite dielectric slab of thickness a, can be expressed as [22]

$$\tan\left[\pi\left(\frac{a}{\lambda_s}\right)\sqrt{(\epsilon_c/\epsilon_s-\epsilon_e/\epsilon_s)}\right]=\frac{\sqrt{(\epsilon_e/\epsilon_s-1)}}{\sqrt{(\epsilon_c/\epsilon_s-\epsilon_e/\epsilon_s)}}. \tag{1}$$

λ_s is the wavelength in the outer dielectric medium, $\epsilon_e = (\beta_p/k_0)^2$ is the effective dielectric constant of the PPDW mode, where β_p is the propagation constant of the PPDW mode, and k_0 is the free-space wavenumber. Fig. 2 shows the dispersion curves of the PPDW mode (fundamental TE_{10} mode) along with those of higher order modes of the guide, computed for $\epsilon_s = 1.0$, and $\epsilon_c = 10.8$. These curves are generated for a specific width-to-height ratio of the central dielectric guide $(a/b = 1)$, but serves to illustrate the general behavior of the fundamental mode in relations to the other higher order modes. As can be seen in Fig. 2, the fundamental

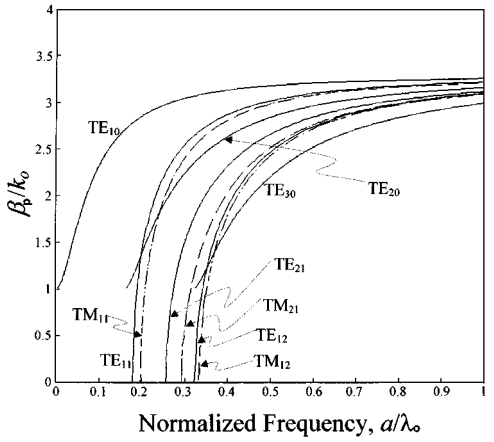

Fig. 2. Dispersion curves for the fundamental PPDW mode (the TE_{10} mode), along with other higher order TE and TM modes of the waveguide structure for $a/b = 1, \epsilon_c = 10.8, \epsilon_s = 1.0$.

TE_{10} mode is the only mode that propagates down to dc. The TM_{10} mode, which requires electric-field components in the z- and y-directions, with no variation in the x-direction, cannot be sustained due to conflicting boundary conditions required on the parallel conducting planes. Using the coordinates described before, the TE_{10} mode has only one component of the electric field E_x and two components of magnetic fields H_y and H_z. Dispersion data and cutoff limits of the higher order modes, similar to those shown in Fig. 2, are used for the analysis and design of the coax-to-PPDW transition in Section III.

As mentioned earlier, the PPDW, unlike printed transmission-line structures with parallel metal planes (striplines, conductor-backed slotline, conductor-backed coplanar waveguide) has a critical advantage of confining power in the central guiding region, without radiating or leaking into the surrounding parallel-plate modes. The parallel metal plates of a PPDW will also serve to provide isolation between two stacked layers in the fabrication of multilayer microwave integrated circuits. As it will be shown, though the fundamental PPDW mode is non-TEM, its field configuration in the central region behaves like a quasi-TEM field with naturally definable voltage and impedance. This feature enables the PPDW to be excited without complex transition arrangements. In fact, the coaxial probe can be simply placed at the center of the dielectric strip with the center conductor of the probe connected to the opposite metal plate (see Fig. 1). Theory and experiments show that, with proper design parameters, radiation loss in such a feeding configuration can be maintained at a negligible level.

III. Coax-to-PPDW Transition Analysis

In order to understand the efficiency of excitation/coupling of a coax-to-PPDW transition, and the input-impedance characteristics, we perform a detailed theoretical analysis using a spectral-domain method. We assume that the PPDW has been properly designed, based on the earlier discussions, to ensure a single-modal operation. The geometry of Fig. 1 is a

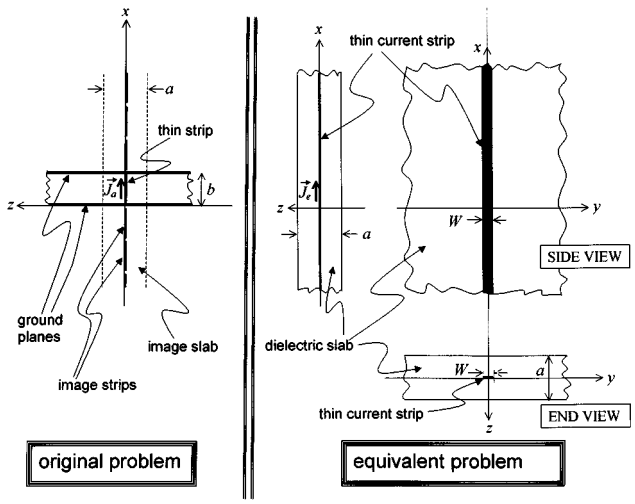

Fig. 3. Geometry of an equivalent problem used for solving a coax-to-PPDW transition. The equivalent geometry is obtained via imaging over the parallel ground planes of the PPDW. The coaxial probe is approximated as a thin strip of an equivalent width. Through imaging, the thin strip is extended into an infinitely long strip of current in the x-direction, placed at the center of a dielectric slab of infinite lateral extent, and thickness a.

three-port circuit (with probe input as one of the ports) and the other two PPDW ports are symmetric to each other. For a complete characterization of the three-port circuit, we first analyze with a current I_0 injected on the probe input, with the other two PPDW ports match terminated (equivalently, having an infinite-long PPDW extending infinitely in both $\pm y$-directions.) In the second step, we excite one of the PPDW ports with an incident PPDW mode having an unit voltage, while the other waveguide port is match terminated, and the probe port is terminated with a short circuit. Under this condition, for simplicity, the waveguide may also be physically extended to an infinite length in both sides. The results of the above two solutions, with proper symmetry considerations to treat excitation from the second PPDW port, will completely describe the coaxial-to-PPDW transition. The two steps of the solution will be presented separately in Sections III-A–III-C.

A. Current Excitation of the Probe

In order to simplify the analysis, we replace the coaxial probe of a cylindrical cross section with a current strip (henceforth, interchangeably referred to as a current strip or probe) of an equivalent width $W = \pi r$, where r is the radius of the cylindrical probe. This should be a reasonable treatment, expected to maintain the essential characteristic trends of the original cylindrical probe. The method of imaging is then applied to the current probe/strip, which leads to an infinite number of reflections about the two parallel metal planes. As a result, the coax-to-PPDW transition geometry of Fig. 1 is transformed into an equivalent problem having an infinitely long strip, embedded halfway inside an infinite dielectric slab of thickness a. The equivalent geometry is shown in Fig. 3. The actual surface current $\vec{J}_a$ on the strip is assumed to flow only along the longitudinal direction x, with uniform magnitude over the width, as

well as the length of the strip. This is known to be a good approximation for narrow strips (or, equivalently, thin probes) and thin PPDWs (small b). Thus, we have

$$\vec{J}_a(x,y) = \begin{cases} \hat{x}\dfrac{I_o}{W}, & |y| \le \dfrac{W}{2};\ 0 < x < b \\ 0, & |y| > \dfrac{W}{2};\ 0 < x < b \end{cases} \tag{2}$$

where the unknown parameter I_o is the total input current into the coaxial probe. After the imaging of the actual current, the equivalent problem, as shown in Fig. 3, can be seen as a ribbon current of infinite extent in the x-direction, of width W in the y-direction, and zero thickness in the z-direction. This infinite current strip $\vec{J}_e$ can be represented as

$$\vec{J}_e(x,y) = \begin{cases} \hat{x}\dfrac{I_o}{W}, & |y| \le \dfrac{W}{2};\ -\infty < x < +\infty \\ 0, & |y| > \dfrac{W}{2};\ -\infty < x < +\infty. \end{cases} \tag{3}$$

In the spectral domain, this equivalent current can be represented as its Fourier transform $\tilde{\vec{J}}_e(k_x,k_y)$

$$\begin{aligned} \tilde{\vec{J}}_e(k_x,k_y) &= \int_{-\infty}^{+\infty} dx \int_{-(W/2)}^{(W/2)} dy \hat{x}\frac{I_o}{W} e^{-j(k_x x + k_y y)} \\ &= 2\pi\delta(k_x) I_o \operatorname{sinc}\left(\frac{k_y W}{2}\right)\hat{x}. \end{aligned} \tag{4}$$

Let $\vec{E}_a$ and $\vec{E}_e$ denote the actual and equivalent electric field generated by the currents $\vec{J}_a$ and $\vec{J}_e$, respectively (Fig. 3). Let $\overset{\cong}{G}_{\vec{E}\vec{J}}$ denote the spectral dyadic Green's function for an electric field $\vec{E}$, produced due to an electric current $\vec{J}$ placed on the x–y-plane of the probe $z = 0$. We can evaluate the electric field due to the current $\vec{J}_e$ as follows:

$$\begin{aligned} \vec{E}_e &= \frac{1}{4\pi^2}\int_{-\infty}^{+\infty} dk_x \int_{-\infty}^{+\infty} dk_y \overset{\cong}{G}_{\vec{E}\vec{J}} \cdot \tilde{\vec{J}}_e e^{j(k_x x + k_y y)} \\ &= \frac{1}{4\pi^2}\int_{-\infty}^{+\infty} dk_x \int_{-\infty}^{+\infty} dk_y \left\{ \overset{\cong}{G}_{\vec{E}\vec{J}} \cdot \hat{x} \right. \\ &\qquad \left. \cdot 2\pi\delta(k_x) I_o \operatorname{sinc}\left(\frac{k_y W}{2}\right) e^{j(k_x x + k_y y)} \right\} \\ &= \frac{1}{2\pi}\int_{-\infty}^{+\infty} dk_y \overset{\cong}{G}_{\vec{E}\vec{J}}(k_x = 0, k_y) \cdot \hat{x} I_o \operatorname{sinc}\left(\frac{k_y W}{2}\right) e^{jk_y y}. \end{aligned} \tag{5}$$

The input impedance Z_{in}, seen at the input of the probe by a delta-gap voltage source, can be expressed in terms of the total complex power P_s, delivered by the current strip

$$\begin{aligned} Z_{\text{in}} &= \frac{P_s}{|I_0|^2} \\ &= -\frac{1}{|I_0|^2}\int_0^b dx \int_{-(W/2)}^{(W/2)} dy \vec{E}_a \cdot \vec{J}_a^* \\ &= -\frac{b}{|I_0|^2}\int_{-(W/2)}^{(W/2)} dy \vec{E}_e \cdot \vec{J}_e^*. \end{aligned} \tag{6}$$

Integration with respect to x has been effected immediately because the integrand is independent of x within region $0 < x < b$.

Also, within the region of the parallel plates, the actual electric field $\vec{E}_a$ produced by the thin current strip is equal to $\vec{E}_e$ of the equivalent problem. Substituting the expression of $\vec{E}_e$ from (5) in (6), and using $\vec{J}_e$ from (3), we have

$$\begin{aligned} Z_{\text{in}} &= -\frac{b}{2\pi|I_0|^2}\int_{-(W/2)}^{(W/2)} dy \left\{ \int_{-\infty}^{+\infty} dk_y \overset{\cong}{G}_{\vec{E}\vec{J}}(k_x = 0, k_y) \right. \\ &\qquad \left. \cdot \hat{x} I_o \operatorname{sinc}\left(\frac{k_y W}{2}\right) e^{jk_y y} \right\} \cdot \left(\hat{x}\frac{I_0^*}{W}\right) \\ &= -\frac{b}{2\pi}\int_{-\infty}^{+\infty} dk_y \left[\overset{\cong}{G}_{\vec{E}\vec{J}}(k_x = 0, k_y) \cdot \hat{x} \operatorname{sinc}\left(\frac{k_y W}{2}\right)\right] \\ &\qquad \cdot \hat{x} \operatorname{sinc}\left(\frac{k_y W}{2}\right) \\ &= -\frac{b}{2\pi}\int_{-\infty}^{+\infty} dk_y \tilde{G}_{E_x J_x}(k_x = 0, k_y) \operatorname{sinc}^2\left(\frac{k_y W}{2}\right) \end{aligned} \tag{7}$$

and

$$[\overset{\cong}{G}_{\vec{E}\vec{J}}(k_x,k_y) \cdot \hat{x}] \cdot \hat{x} = \widetilde{G}_{E_x J_x}(k_x,k_y). \tag{8}$$

$\widetilde{G}_{E_x J_x}(k_x,k_y)$ is the spectral Green's function component for the x-directed electric field on the $z = 0$ plane, produced due to a x-directed electric current placed on the same plane. The medium under consideration is the dielectric slab of the equivalent structure of Fig. 3, with thickness a. Both the dielectric slab and current strip are parallel to the x–y-plane. The Green's function $\widetilde{G}_{E_x J_x}(k_x,k_y)$ of the equivalent problem can be found from the multilayer Green's function approach of [23], [24]

$$\begin{aligned} \tilde{G}_{E_x J_x}(k_x = 0, k_y) &= -\left(\frac{\omega\mu}{2\beta_1}\right) \\ &\quad \times \left(\frac{\beta_1 \cos(\beta_1 a/2) + j\beta_2 \sin(\beta_1 a/2)}{j\beta_1 \sin(\beta_1 a/2) + \beta_2 \cos(\beta_1 a/2)}\right) \end{aligned} \tag{9}$$

$$\beta_1 = \sqrt{k_o^2 \epsilon_c - \alpha^2} \tag{10}$$

$$\beta_2 = \sqrt{k_o^2 \epsilon_s - \alpha^2}, \qquad \operatorname{Im}(\beta_2) < 0 \tag{11}$$

$$\alpha^2 = k_x^2 + k_y^2 = k_y^2. \tag{12}$$

Substituting the Green's function of (9) into (7), we obtain the following spectral integral for the input impedance of the coaxial probe:

$$\begin{aligned} Z_{\text{in}} = \frac{b}{4\pi}\int_{-\infty}^{+\infty} &\left(\frac{\omega\mu}{\beta_1}\right)\left(\frac{\beta_1 \cos(\beta_1 a/2) + j\beta_2 \sin(\beta_1 a/2)}{j\beta_1 \sin(\beta_1 a/2) + \beta_2 \cos(\beta_1 a/2)}\right) \\ &\times \operatorname{sinc}^2\left(\frac{k_y W}{2}\right) dk_y. \end{aligned} \tag{13}$$

This integral is evaluated numerically, but care must be given in order to deform the contour around the singularities of the Green's function, and include the resulting residue contributions. It can be shown that, under the condition of a single-modal operation of the PPDW, the Green's function $\widetilde{G}_{E_x J_x}(k_x = 0, k_y)$ has a pair of singular points $k_y = \pm\beta_p$ on the real axis. $\beta_p = k_0\sqrt{\epsilon_e}$ is the propagation constant of the PPDW waveguide mode, which is same as the fundamental TE_{10} mode of the dielectric slab structure in the equivalent problem of Fig. 3. The residue contribution Z_{res} can be found analytically, and

then added to the rest of the principal-value integration Z_e obtained numerically as follows:

$$Z_{\text{in}} = Z_{\text{res}} + Z_e. \tag{14}$$

In order to avoid any numerical difficulties in computing the principal-value integration, it may be useful to extract out the singular part [1], [2] [25] from the integrand, leaving a well-behaved smooth function for convenient numerical integration. Applying residue calculus to (13) [26], the residue contribution Z_{res} can be derived and simplified as

$$Z_{\text{res}} = -bj\,\text{sinc}^2\left(\frac{\beta_p W}{2}\right)\,\text{Res}\left[\widetilde{G}_{E_x J_x}\,(k_x=0,k_y)\right]_{k_y=-\beta_p} \tag{15}$$

$$= \text{sinc}^2\left(\frac{\beta_p W}{2}\right)\left(\frac{\pi\eta_0 b}{\lambda_0}\right)\left(\frac{\sqrt{1-(\epsilon_s/\epsilon_e)}}{1+\frac{a}{\lambda_0}\pi\sqrt{\epsilon_e-\epsilon_s}}\right) \tag{16}$$

where $\epsilon_e = (\beta_p/k_o)^2$ is called the effective dielectric constant of the TE_{10} mode, η_o is free-space wave impedance, and λ_0 is the free-space wavelength. The width W of the strip (or, equivalently, the diameter of the probe) is normally much smaller than $(\lambda/\sqrt{\epsilon_e})$, such that $(\beta_p W/2) \ll 1$. Under this condition, for all practical purposes, the sinc^2 function in (16) can be approximated as unity. Consequently, the expression of Z_{res} in (16) may be approximated as

$$Z_{\text{res}} \simeq \left(\frac{\pi\eta_0 b}{\lambda_0}\right)\left(\frac{\sqrt{1-(\epsilon_s/\epsilon_e)}}{1+\frac{a}{\lambda_0}\pi\sqrt{\epsilon_e-\epsilon_s}}\right). \tag{17}$$

The residue part Z_{res} can be interpreted as due to the excitation of the TE_{10} surface-wave mode of the dielectric slab in the equivalent structure of Fig. 3, which corresponds to the excitation of the PPDW guided mode in the original structure of Fig. 1. It may be seen from (17) that Z_{res} is a real number for lossless dielectrics with $\epsilon_s < \epsilon_e < \epsilon_c$. The principal-value contribution Z_e, on the other hand, is a complex number with both real and imaginary parts:

$$Z_e = R_{\text{rad}} + jX_{\text{coax}}. \tag{18}$$

The real part R_{rad} is contributed by the power radiated into the top and bottom open media in Fig. 3 or, equivalently, to the parallel-plate mode in the medium surrounding the PPDW (with dielectric constant ϵ_s). Hence, R_{rad} amounts to undesired loss, in contrast to Z_{res}, which is attributed to useful guided-mode power excited in the PPDW. The imaginary part of the impedance X_{coax} determines the additional reactive loading produced by the coaxial probe. We may define the efficiency ρ of the transition as the ratio of the useful guided power to the total power excited by the probe as follows:

$$\rho = \frac{Z_{\text{res}}}{Z_{\text{res}} + R_{\text{rad}}}. \tag{19}$$

The above definition is applicable for a two-sided excitation, as shown in Fig. 1. For an excitation to one side of the PPDW guide, while the other side is stub terminated, the efficiency will be different depending on the stub reactance. In that case, one needs to use an appropriate circuit model, to be developed in the following sections, in order to account for the effect of any termination on the total circuit efficiency.

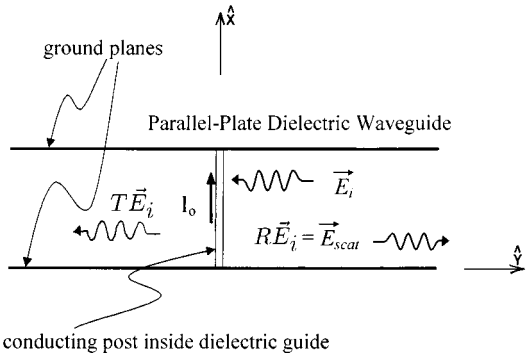

Fig. 4. PPDW mode with electric field $\vec{E}_i$, incident on a coaxial probe located at the center of the PPDW. The other port of the PPDW is match terminated. The input port of the probe is short circuited, allowing an induced current $\hat{x}I_0$ to flow on the conducting probe.

B. Incidence From a PPDW Port

Fig. 4 shows the situation when one of the PPDW ports is excited by an incoming TE_{10} wave, i.e., $\vec{E}_i e^{j\beta_p y}$, while the second waveguide port is match terminated and the probe input is terminated with a short circuit. As shown in Fig. 4, a current I_0 is induced on the probe, assumed in the $\hat{x}$-direction (see Figs. 1 and 3 for coordinates), which produces the reflected field $R\vec{E}_i e^{-j\beta_p y}$ returning back to the input port. Due to symmetry, an outgoing scattered field $R\vec{E}_i e^{j\beta_p y}$ of the same magnitude as the reflection is also produced at the second PPDW port. This adds to the incident field $\vec{E}_i e^{j\beta_p y}$ to constitute the total transmitted field $T\vec{E}_i e^{j\beta_p y}$, resulting in the following relationship:

$$T = 1 + R. \tag{20}$$

For convenience, let us normalize the incident field $\vec{E}_i$, such that the incident voltage V_i is -1 V (positive E_{xi}) as follows:

$$V_i = -bE_{xi}(z=0) = -1 \tag{21}$$

or, in other words, the x component of the electric field E_{xi} of the incident wave, at the center of the PPDW ($z = 0$ plane), is equal to $1/b$ V/m. Let us find the guided-wave electric fields, propagating in the $+y$-direction, produced due to the induced current $\hat{x}I_0$ on the probe. The x component of this field can be equated to that of the reflected wave $\text{RE}_{xi} = R/b$ V/m. This problem can be treated using the same formulation used earlier for the first part of the analysis in Section III-A. The equation of the electric field $\vec{E}_e$ in (5) can be used here again. If only the guided-wave part of the field, propagating to the input port (with a variation $e^{-j\beta_p y}$) is needed, residue theory can be applied to (5). Taking only the x component of (5), and properly deriving the residue contribution, we obtain

$$\text{RE}_{xi} = jI_0\,\text{sinc}\left(\frac{\beta_p W}{2}\right) \times \text{Res}\left[\widetilde{G}_{E_x J_x}\,(k_x=0,k_y)\right]_{k_y=-\beta_p} = \frac{R}{b}. \tag{22}$$

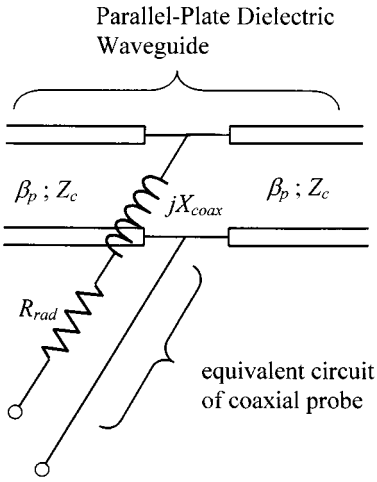

Fig. 5. Equivalent circuit of the coaxial-to-PPDW transition of Fig. 1.

Now, comparing the expression of $Z_{\rm res}$ in (16) with (22), and approximating the above sinc function to unity for small W, the following simple relationship between $I_0, R,$ and $Z_{\rm res}$ can be obtained:

$$R = -I_0 Z_{\rm res}. \tag{23}$$

In addition, the boundary condition on the conducting post must be ensured as follows:

$$\vec{E}_e + \vec{E}_i e^{j\beta_p y} = 0, \qquad 0 \le x \le b; \quad |y| \le \frac{W}{2} \tag{24}$$

where $\vec{E}_e$ is the scattered field (of the image equivalent problem) due to the induced probe current $\hat{x}I_0$. This condition can be enforced by a testing procedure in the following form:

$$\int_0^b dx \int_{-(W/2)}^{(W/2)} dy \vec{E}_e \cdot \vec{J}_e^* + \int_0^b dx \int_{-(W/2)}^{(W/2)} dy \vec{E}_i \cdot \vec{J}_e^* = 0. \tag{25}$$

Using (3), (6), and (21) in (25), we can obtain the following relationship between the input impedance $Z_{\rm in}$, seen by the probe in the first part of the solution (in Section III-A) and the current I_0, now induced on the probe:

$$-Z_{\rm in}|I_o|^2 + I_0^* = 0 \quad I_0 = \frac{1}{Z_{\rm in}}. \tag{26}$$

The unknown current I_0 may be eliminated from (23) and (26) to obtain

$$R = -\frac{Z_{\rm res}}{Z_{\rm in}}. \tag{27}$$

C. Equivalent Circuit

The two-part analysis presented above in Sections III-A and III-B provides a complete representation of the coax-to-PPDW transition. Based on all the governing equations, i.e., (14), (18), (20), and (27), we can derive an equivalent circuit for the coax-to-PPDW transition of Fig. 1. The equivalent circuit is shown in Fig. 5. For the circuit of Fig. 5 to be consistent with (14), (18), (20), and (27), the value of the characteristic impedance Z_c of the PPDW is required to be approximately twice that of $Z_{\rm res}$. A simple transmission-line circuit theory may be used to verify the following:

$$Z_c = 2Z_{\rm res}. \tag{28}$$

This relationship, together with the expression of $Z_{\rm res}$ in (17), provides the following design equation for the characteristic impedance Z_c of the PPDW, normalized to $\eta_0(b/\lambda_0)$:

$$\frac{Z_c}{\eta_0 \frac{b}{\lambda_0}} = \frac{2Z_{\rm res}}{\eta_0 \frac{b}{\lambda_0}} \simeq 2\pi \frac{\sqrt{1-\epsilon_s/\epsilon_e}}{1+\frac{a}{\lambda_s}\pi\sqrt{\epsilon_e/\epsilon_s - 1}}. \tag{29}$$

Once the effective dielectric constant ϵ_e is known from (1), the normalized expression of the characteristic impedance in (29) can be computed independent of any specific value of the guide thickness b. Observe that the characteristic impedance varies proportionally with thickness b. This allows design of higher levels of impedance just by increasing the substrate thickness b. However, the upper limit for b is constrained by conditions for higher order mode excitation.

It is useful to show that the above expression (29) of the characteristic impedance also follows a power–voltage definition

$$Z_c = \frac{P}{V^2} \tag{30}$$

where P is the total cross-sectional power and V is the integration of the electric field across the parallel plates, computed along the center of the guide $(z = 0)$ (equivalent voltage). For the PPDW mode, the fields have no variation in the x-direction and, thus, the voltage V can be simply calculated as $V = -bE_x$. By deriving the field expressions for the PPDW mode ($\rm TE_{10}$ mode) and using the propagation constant of the guide from (1), P can derived as the integration of $E_x H_z^*$ over the cross section. The expression of P can then be used in (30) and simplified to show that the same expression of Z_c as in (29) is obtained. It may be mentioned here that the power–voltage definition (30) of the characteristic impedance is commonly used for TEM or quasi-TEM transmission lines. Though the PPDW mode is not a TEM or quasi-TEM mode, in this respect, the PPDW line may be treated like a TEM transmission line for circuit modeling purposes.

IV. Results

First, we present results for the equivalent characteristic impedance of the PPDW from (29), as "seen" by a coaxial transition. In Fig. 6, we have a plot of the normalized value of $Z_c = 2Z_{\rm res}$, as a function of $(a/\lambda_s) = (a/\lambda_0)$, with $\epsilon_c = 10.8$ and $\epsilon_s = 1.0$. The cutoff boundaries of the $\rm TE_{20}$ and $\rm TE_{30}$ modes are also shown in Fig. 6 in order to identify regions of single-modal and multimodal operation. The $\rm TE_{20}$ and $\rm TE_{30}$ modes begin to propagate when $(a/\lambda_0) \ge 0.16$ and $(a/\lambda_0) \ge 0.32$, respectively, independent of the substrate thickness b. The cutoff frequency of the $\rm TE_{11}$ mode, however, is a function of the ratio a/b, and will determine proper design of the thickness b in order to avoid the $\rm TE_{11}$ mode. It may be seen from Fig. 6 that, for any desired value of the characteristic impedance, there are, in general, two possible values of a that can meet such a requirement. The characteristic impedance peaks at around $(a/\lambda_0) = 0.044$. In this region of (a/λ_0), the

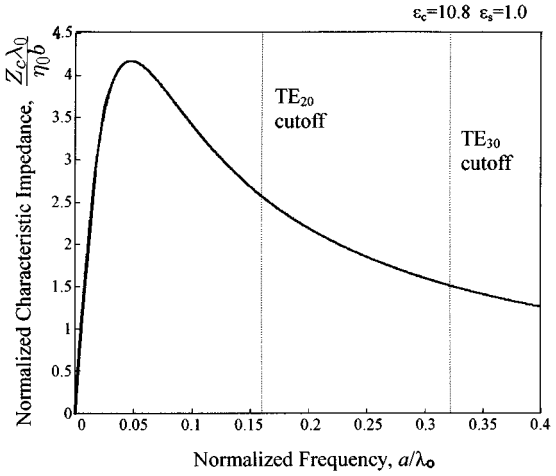

Fig. 6. Characteristic impedance of a PPDW, normalized to $(\eta_0 b/\lambda_0)$, computed as a function of (a/λ_0), showing cutoff ranges for higher order modes.

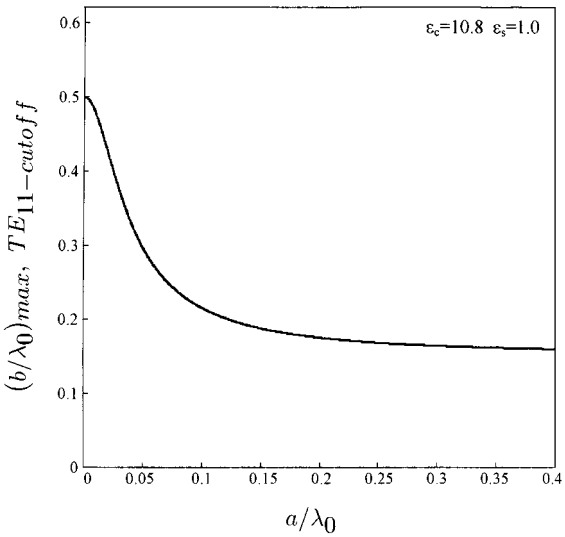

Fig. 8. $(b/\lambda_0)_{\max}$ for TE_{11} cutoff versus (a/λ_0) for the PPDW of Fig. 7.

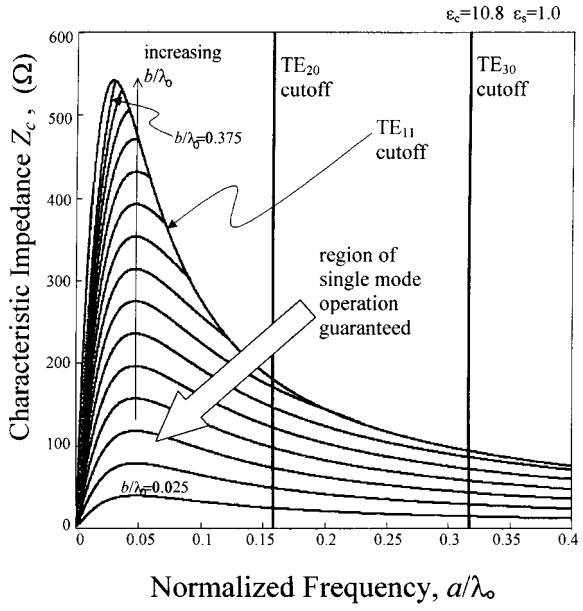

Fig. 7. Design data for the characteristic impedance of a PPDW, plotted for different values of b/λ_0 in increments of $\Delta(b/\lambda_0) = 0.025$. The upper limit for the characteristic impedance is governed by the TE_{11} cutoff. The TE_{20} and TE_{30} cutoff limits are also shown, which limit the maximum value of (a/λ_0) that can be used. The region of single-modal operation is shown.

characteristic impedance is relatively less sensitive to a and/or λ_0, which may be useful for an optimum-bandwidth design.

In Fig. 7, we plot the characteristic impedance for different values of (b/λ_0) (in increments of 0.025), also showing the region of excitation of the TE_{11} mode in addition to the TE_{20} and TE_{30} modes. As mentioned, the characteristic impedance increases proportionally with (b/λ_0). However, for a given value of (a/λ_0), there is a maximum value of (b/λ_0) and, hence, a maximum limit for the characteristic impedance, which can be used without exciting the TE_{11} mode. This maximum limit of (b/λ_0) is shown in Fig. 8, which using the TE_{11} limits for the characteristic impedance in Fig. 7 have been calculated. For $\epsilon_c = 10.8$ and $\epsilon_s = 1.0$, the absolute maximum value of characteristic impedance one can obtain is approximately 550 Ω, which corresponds to $(b/\lambda_0) = 0.375$ and $(a/\lambda_0) = 0.027$.

In Fig. 7, single-modal operation is normally guaranteed in the region limited by the TE_{20} and TE_{11} modes. However, in applications where there is even symmetry of the electric field about the $z = 0$ plane, the mode TE_{20} (which requires an odd symmetry of E_x about $z = 0$) will not be excited. Under such circumstances, the region limited by the TE_{30} and TE_{11} modes can be considered the practical range of single-modal operation. Consequently, under the physical symmetry, more flexibility is exercised in the design of the characteristic impedance. For a probe-to-PPDW transition, the probe is ideally placed at the center of the guide $(z = 0)$, which means the electric field has an even symmetry about the $z = 0$ plane. Therefore, Fig. 7 may be used to design the PPDW covering a broader range of parameters, limited by the TE_{30} mode, not by the TE_{20} mode.

Following the derivation presented in Section III, we computed $Z_{\mathrm{res}}, R_{\mathrm{rad}}$, and efficiency ρ [as defined in (19)] as a function of (a/λ_0) for $\epsilon_c = 10.8$ and $\epsilon_s = 1.0$. The results are shown in Fig. 9 with Z_{res} and R_{rad} normalized with respect to $(\eta_0 b/\lambda_0)$. It can be seen that the efficiency attains a maximum of about 95% for $0.05 < (a/\lambda_0) < 0.2$. This suggests, in order to design an efficient coaxial transition, one should design the PPDW to operate in the above range of (a/λ_0). Notice that in the absence of the PPDW (equivalently $(a/\lambda_0) = 0$), there is significant radiation, which is successfully suppressed to a very low level by the PPDW due to total reflection from the dielectric interfaces.

Fig. 10 shows the normalized reactance X_{coax} of the transition of Fig. 9, but with different values of (W/λ_0). The reactance is seen to exhibit rather weak variation with respect to the width a of the PPDW, except when a is too small. This is expected because X_{coax} is contributed by the reactive near fields of the coaxial probe, which is dominantly affected by the medium in the immediate vicinity of the probe. However, when a is too small, the probe tends to "see" the air, which results

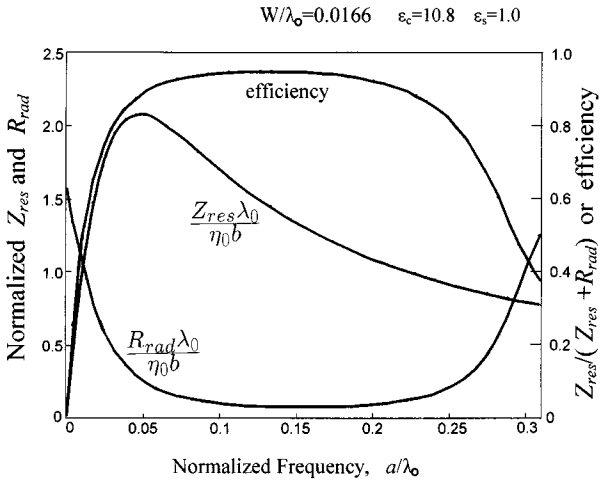

Fig. 9. Computed design data for the real parts of the input impedances $Z_{\rm res}$ and $R_{\rm rad}$ normalized to $(\eta_0 b/\lambda_0)$, as seen by the input probe, plotted as a function of a/λ_0. A reasonable value of $W/\lambda_0 = 0.017$ is used in the calculations. $Z_{\rm res}$ is contributed due to excitation of the guided wave along the PPDW, whereas $R_{\rm rad}$ is the due to radiation loss into the parallel-plate mode in the surrounding medium. The data for the efficiency of excitation, as defined in (19), is also plotted, showing a maximum of approximately 95% for a double-sided excitation.

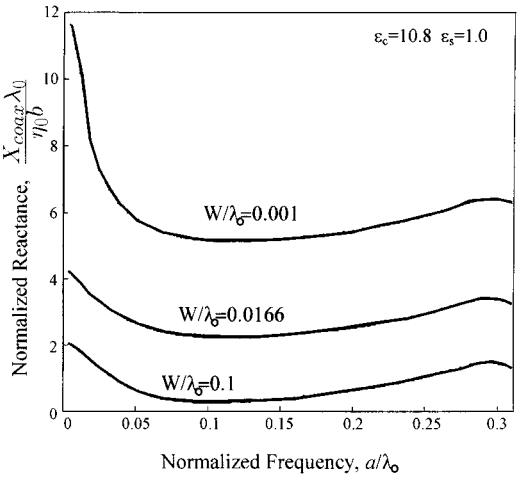

Fig. 10. Computed values of normalized $X_{\rm coax}$ for the probe transition of Fig. 9, plotted as a function of a/λ_0. Data for three different values of W/λ_0 are plotted for comparison.

in an increase of the reactance, as seen in Fig. 10. The probe reactance would also change significantly for very large values of a/λ_0, due to excitation of higher order modes. However, we have limited the maximum data range in Fig. 10 to $a/\lambda_0 < 0.3$, where the PPDW supports a single mode, which is of practical interest here.

It is useful to establish an equivalence between the radius r of a cylindrical probe and the width W of a flat strip that we are considering here. We observe the reactance in Fig. 10 for a metal strip in a PPDW, in the region $0.1 < a/\lambda_0 < 0.2$, where it is more or less insensitive to the guide width a, as explained above. It is meaningful to compare this reactance to that of a cylindrical probe in a uniform parallel-plate medium with the same $\epsilon_r = 10.8$. This is a simpler problem, which we have separately solved using a standard analysis [14], assuming current flow only on the surface of the cylinder. Consider, for example, the data for $W/\lambda_0 = 0.0166$, where the normalized reactance in the central range of a/λ_0 is $(X_{\rm coax}\lambda_0/\eta_0 b) \simeq 2.3$. The same level of the normalized reactance we obtained from a cylindrical probe in a uniform medium having $r/\lambda_0 \simeq 0.005$. This establishes an estimate for the ratio between equivalent r and W:$(W/r) \simeq (0.0166/0.005) = 3.32$. This ratio is close to π, which means the equivalent width W for the uniform current strip is close to πr or about half of the circumference of the cylindrical probe. This is sensible, as one would normally guess/estimate. The equivalent width W is found to be somewhat larger $(W \simeq 4r)$ if one treats the current distribution on the strip more rigorously, having a realistic edge-condition at the strip edges, instead of the uniform current distribution assumed here [15]. However, once a suitable equivalence is established, all basic characteristic trends for a cylindrical probe in a PPDW is expected to follow those we have computed for the equivalent strip excitation.

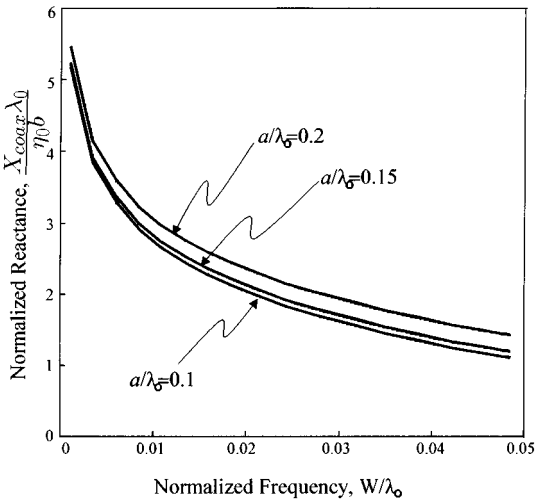

Fig. 11. Normalized $X_{\rm coax}$ for the same parameters of Fig. 10, but plotted as a function of (W/λ_0) for three values of a/λ_0 (=$0.1, 0.15$, and 0.25).

The variation of the reactance as a function of the normalized width (W/λ_0) of the probe is shown in Fig. 11, for different values of the guide width a/λ_0. Consistent with Fig. 10, the reactance in Fig. 11 shows relative insensitivity to (a/λ_0) in the range $0.1 < (a/\lambda_0) < 0.2$. In addition, the reactance is seen to rapidly increase for too narrow probes, which suggests the use of such narrow probes should be avoided. The trend is seen to be logarithmic for narrow W, which is consistent with that expected for a probe with small r.

A. Experiment

Fig. 12 shows the geometry of a prototype coaxial-PPDW-coaxial transition that we have designed and fabricated. The PPDW is designed with a width $a = 14.4$ mm, thickness $b = 5.08$ mm, and dielectric constant $\epsilon_c = 10.8$ for the central guide. The outside dielectric is air (i.e., $\epsilon_s = 1.0$). From Fig. 7, this set of parameters is selected to provide a characteristic impedance of approximately 50 Ω, at the design frequency of 2.5 GHz, for convenient matching to 50-Ω input ports. Metal plates are used to form short-circuit planes for the PPDW, using which short-circuit stubs are made for tuning. The stub lengths $L1 = L2$ are designed to be quarter-wavelength guides at 2.5 GHz,

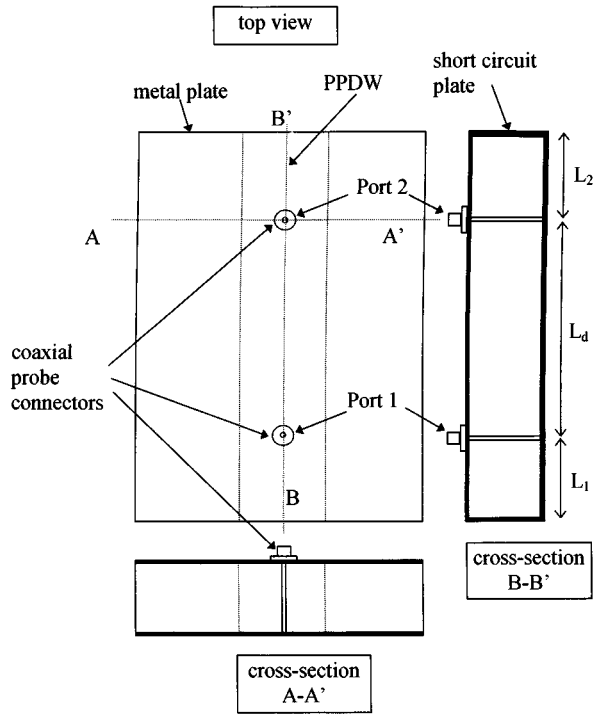

Fig. 12. Prototype geometry of a two-port coax-PPDW-coax transition used for experiment.

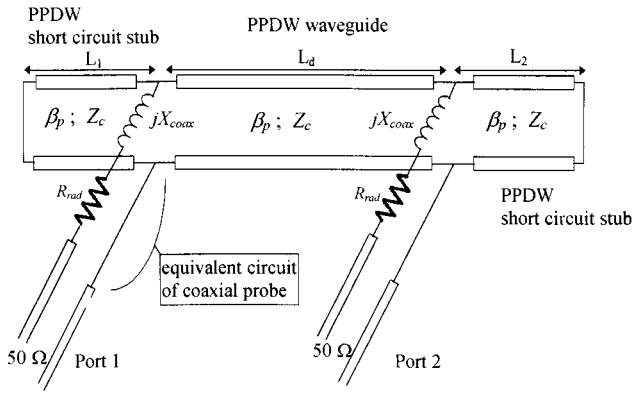

Fig. 13. Equivalent circuit for the coax-PPDW-coax transition of Fig. 12.

in order to result in open circuits at the planes of the coaxial probes.

The equivalent circuit of Fig. 5 for a single transition is extended in Fig. 13 to provide an equivalent circuit for the two-port prototype of Fig. 12. The probe reactance $X_{\rm coax}$ and the radiation resistance $R_{\rm rad}$ rigorously account for the effect of the probe. $X_{\rm coax}, R_{\rm rad}$, and $Z_{\rm res}$ (which is about half of the characteristic impedance Z_c) for the prototype design are computed over the frequency range of 2–3 GHz, as shown in Fig. 14. The actual coaxial probe is cylindrical in shape with a diameter $d = 1.27$ mm. As discussed in Section III, the width W of the equivalent strip used in our model is $(\pi/2)d$. It can be seen in Fig. 14 that $R_{\rm rad}$ is less than 1.5 Ω, compared to the guided-wave impedance $Z_{\rm res}$ of approximately 25 Ω, which translates to an expected value of about 97% (0.13 dB) for the efficiency [$=2Z_{\rm res}/(2Z_{\rm res}+R_{\rm rad})$ for a single-sided excitation] of excitation for a single transition.

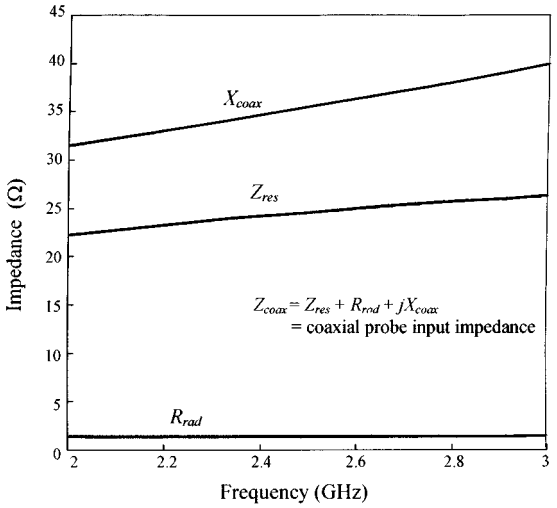

Fig. 14. Real and imaginary parts of the equivalent impedance of each coaxial-to-PPDW transition used in the prototype geometry. PPDW dimensions: $a = 14.4$ mm, $b = 5.08$ mm, $\epsilon_c = 10.8, \epsilon_s = 1.0$. Diameter of coaxial probe $= 1.27$ mm. Width of the equivalent strip approximation $W = (1.27\pi/2)$ mm.

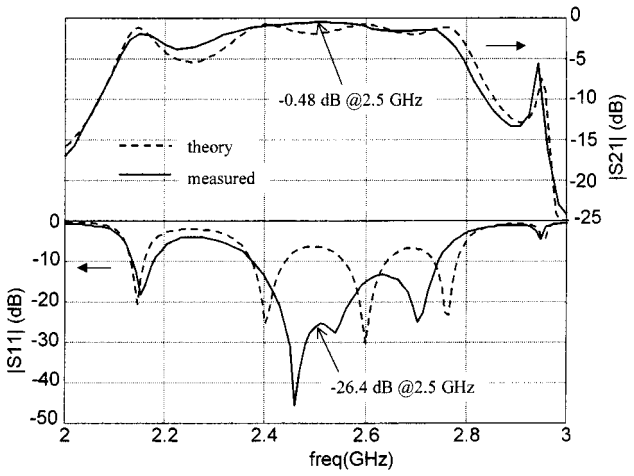

Fig. 15. Measured and computed (*top*) insertion loss and (*bottom*) return loss of the prototype coax-PPDW-coax transition. PPDW dimensions: $a = 14.4$ mm, $b = 5.08$ mm, $\epsilon_c = 10.8, \epsilon_s = 1.0$. Stub lengths $L1 = L2 = 38$ mm. Length of the connecting PPDW $Ld = 140$ mm. Loss tangent of the central dielectric $= .0028$, metal conductivity (brass) $= 1.58e7$ S/m.

The insertion loss or S_{21} of the coax-PPDW-coax transition is measured on a network analyzer, and the results are compared with the theoretical computation in Fig. 15 (top) (insertion loss) and Fig. 16 (Smith chart plot of S_{21}). There is good agreement between the theory and experiments in both magnitude and phase, which follow most of the characteristic features. For a proper evaluation of the performance of the prototype, we have also included in the calculations the material loss due to the metal and dielectric media, using available values of the conductivity or loss tangent of the respective media (through a perturbation model of loss). This is because the length of the PPDW between the two ports of the prototype is significant in order for the loss to be ignored. Calculated S_{21} with material loss is found to be -1.89 dB at 2.5 GHz, while calculated S_{21} without loss is -1.52 dB. This amounts to approximately 0.37

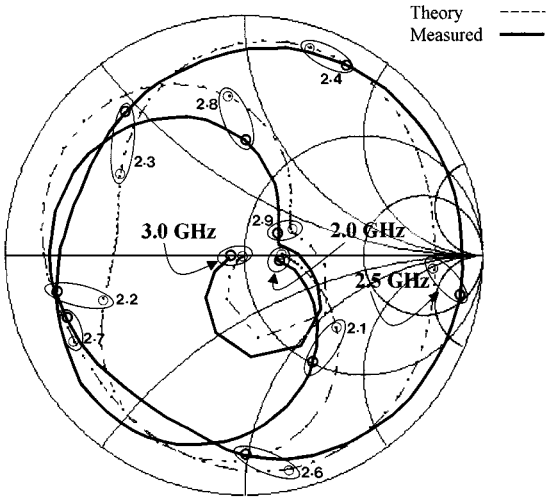

Fig. 16. Measured and computed Smith chart plot of S_{21} for the geometry of Fig. 15.

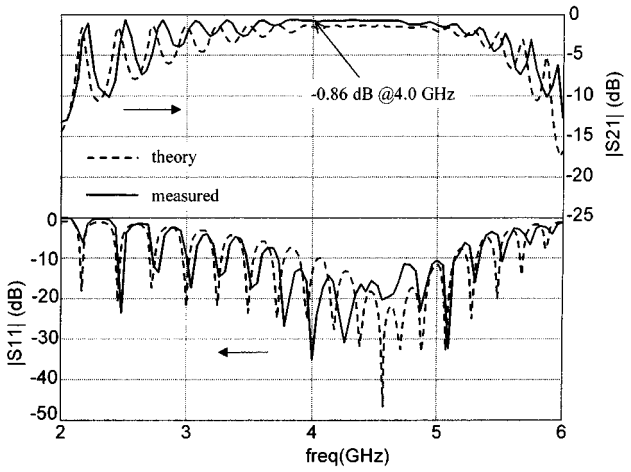

Fig. 17. Measured and computed (*top*) insertion loss and (*bottom*) return loss of a prototype coax-PPDW-coax transition, designed with a narrower guide width a and a smaller guide thickness b, compared to those for Fig. 15. PPDW dimensions: $a = 5$ mm, $b = 2.54$ mm, $\epsilon_c = 10.8, \epsilon_s = 1.0$. Stub lengths $L1 = L2 = 10$ mm. Length of the connecting PPDW $Ld = 225$ mm. Loss tangent of the central dielectric $= .0028$, metal conductivity (brass) $= 1.58e7$ S/m.

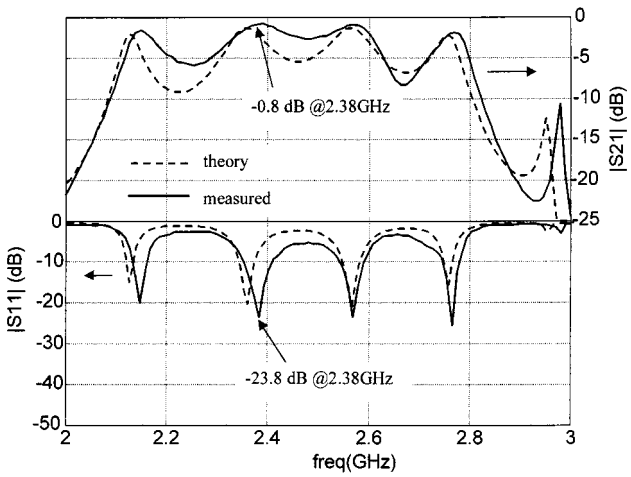

Fig. 18. Measured and computed (*top*) insertion loss and (*bottom*) return loss of a prototype coax-PPDW-coax transition, designed with the same guide width a, but a smaller guide thickness b compared to those for Fig. 15. PPDW dimensions: $a = 14.4$ mm, $b = 2.54$ mm, $\epsilon_c = 10.8, \epsilon_s = 1.0$. Stub lengths $L1 = L2 = 38$ mm. Length of the connecting PPDW $Ld = 140$ mm. Loss tangent of the central dielectric $= .0028$, metal conductivity (brass) $= 1.58e7$ S/m.

dB of loss in the conductor and dielectric strip of the waveguide itself. Measurement at 2.5 GHz shows approximately 0.48 dB of total insertion loss. If one excludes the above calculated material loss of 0.37 dB in the waveguide, the experimental value of 0.48 dB translates to 0.11 dB of total insertion loss due to the two coaxial probes at the two ports or, equivalently, to only 0.055 dB (negligible) of radiation loss per one coaxial probe. This may be compared to the estimated value of approximately 0.13 dB from computation, which was discussed earlier.

Notice in Fig. 15 (top) that the experimental value of insertion loss at 2.5 GHz is actually better than the calculated value by approximately 1.5 dB. The difference is due to standing waves in the PPDW produced by input mismatch, not due to differences in predicting the power loss. This may be evident from the rippling trend in the computed insertion-loss result of Fig. 15 (top), which is a typical behavior under input mismatch. We attribute it to inaccuracy in computation of the probe reactance and to errors in the fabrication. The input return loss for the geometry is seen in Fig. 15 (bottom). The rippling differences in the insertion loss data of Fig. 15 (top) translate to the more pronounced deviations (due to decibel scale) in the return-loss data of Fig. 15 (bottom).

To study the probe reactance further, we repeated similar procedures to design and test two more prototypes of coax-PPDW-coax transitions, having different sets of guide width a and guide thickness b. For both of these cases, we chose a smaller guide thickness $b = 2.54$ mm, which is half of that for Fig. 15. The first prototype is designed with approximately 50-Ω characteristic impedance, but with a narrower width of $a = 5.0$ mm, while the second prototype is designed with approximately 25-Ω characteristic impedance with a wider width of $a = 14.4$ mm. The insertion loss and return loss results for the first case are shown in Fig. 17 (top) and Fig. 17 (bottom), and for the second case in Fig. 18 (top) and Fig. 18 (bottom), respectively. As with the insertion loss results of Fig. 15 (top), we also see good agreement between theory and experimental data for the insertion loss in both Figs. 17 (top) and 18 (top). The best insertion loss achieved in both cases over the frequency range of observation is approximately 0.8 dB. However, unlike the return-loss results of Fig. 15 (bottom), we have closer agreement between the theory and experimental data for return loss in both Figs. 17 (bottom) and 18 (bottom). The probe analysis and/or the circuit model seem to be more accurate for the thinner guides of Figs. 17 and 18. For a thicker guide, one may need to account for higher order current variation along the probe for accurate modeling of the probe reactance. One may also need to account for higher order evanescent coupling between the probe transition and any nearby termination at one end of the PPDW. It may be noted that such evanescent coupling is not included in the circuit model of Fig. 5.

V. Conclusion

We have shown for the first time that, when properly designed, a coaxial-to-PPDW transition can be used as a simple and efficient method of exciting the PPDW. This is contrary to some misconception in the past that any transition in the fundamental TE_{10} mode of a PPDW would be too inefficient due to severe radiation to its surrounding parallel-plate medium. We conducted a theoretical investigation of the coaxial transition using a spectral-domain formulation, by approximating the probe as a thin conducting strip. Useful design data for the radiation loss, efficiency, and input impedance of the coaxial transition were computed. Based on the theoretical data, experimental prototypes of two-port circuits, consisting of two coaxial transitions at the two ends of a PPDW guide, were designed and tested. As the experimental and theoretical results indicate, with proper design, an insertion loss on the order of 0.1 dB could be achieved from a single coaxial-to-PPDW transition. Good agreement between the theory and experiment confirmed the validity and accuracy of the analysis and design data. More accurate models may be needed for modeling a probe transition in a thicker guide (larger b), which accounts for higher order current excitation and coupling effects. Design of such simple transitions is expected to facilitate the use of the PPDW as an efficient transmission medium in multilayer integrated circuits of the future, covering a range of microwave and millimeter-wave frequencies. Conventional printed strip transmission lines are known to be troublesome in such a multilayer environment due to severe excitation of the parallel-plate mode at circuit transitions.

References

[1] N. K. Das and D. M. Pozar, "Multiport scattering analysis of multilayered printed antennas fed by multiple feed ports: Part I—Theory," *IEEE Trans. Antennas Propagat.*, vol. 40, pp. 469–481, May 1992.

[2] ——, "Multiport scattering analysis of multilayered printed antennas fed by multiple feed ports: Part II—Applications," *IEEE Trans. Antennas Propagat.*, vol. 40, pp. 482–491, May 1992.

[3] ——, "Full-wave spectral-domain computation of material, radiation and guided wave losses in infinite multilayered printed transmission lines," *IEEE Trans. Microwave Theory Tech.*, vol. 39, pp. 54–63, Jan. 1991.

[4] D. Nghiem, J. T. Williams, and D. R. Jackson, "Leakage of the dominant mode on stripline with a small air gap," *IEEE Trans. Microwave Theory Tech.*, vol. 43, pp. 2549–2556, Nov. 1995.

[5] N. K. Das, "Methods of suppression or avoidance of parallel-plate leakage from conductor-backed transmission lines," *IEEE Trans. Microwave Theory Tech.*, vol. 44, pp. 169–181, Feb. 1996.

[6] N. K. Das, H. Herscovici, G. Kwan, and D. M. Bolle, "Multilayer integration of microwave and millimeter-wave circuits: New interconnect methods and design considerations," in *Directions for the Next Generation of MMIC Devices and Systems*, N. K. Das and H. L. Bertoni, Eds. New York: Plenum, 1997, pp. 83–96.

[7] F. J. Tischer, "H guide with laminated dielectric slab," *IEEE Trans. Microwave Theory Tech.*, vol. MTT-18, pp. 9–15, Jan. 1970.

[8] T. Yoneyama and S. Nishida, "Nonradiative dielectric waveguide for millimeter-wave integrated circuits," *IEEE Trans. Microwave Theory Tech.*, vol. MTT-29, pp. 1188–1192, Nov. 1981.

[9] L. Han, K. Wu, and R. G. Bosisio, "An integrated transition of microstrip to nonradiative dielectric waveguide for microwave and millimeter-wave circuits," *IEEE Trans. Microwave Theory Tech.*, vol. 45, pp. 1091–1096, July 1996.

[10] D. M. Pozar, "Input impedance and mutual coupling of rectangular microstrip antennas," *IEEE Trans. Antennas Propagat.*, vol. AP-30, pp. 1991–1996, Nov. 1982.

[11] W. J. Tsay and J. T. Aberle, "Analysis of a microstrip line terminated with a shorting pin," *IEEE Trans. Microwave Theory Tech.*, vol. 40, pp. 645–651, Apr. 1992.

[12] J. T. Aberle, D. M. Pozar, and C. R. Birtcher, "Evaluation of input impedance and radar cross section of probe-fed microstrip patch elements using an accurate feed model," *IEEE Trans. Antennas Propagat.*, vol. 39, pp. 1691–1696, Dec. 1991.

[13] J. X. Zheng and D. C. Chang, "End correction network of a coaxial probe for microstrip patch antennas," *IEEE Trans. Antennas Propagat.*, vol. 39, pp. 115–117, Jan. 1991.

[14] R. E. Collin, *Field Theory of Guided Waves*, 2nd ed. New York: IEEE Press, 1991.

[15] N. Marcuvitz, *Waveguide Handbook*. Stevenage, U.K.: Peregrinus, 1986, ch. 5.11.

[16] M. E. Bialkowski and P. J. Khan, "Determination of the admittance of a general waveguide-coaxial line junction," *IEEE Trans. Microwave Theory Tech.*, vol. MTT-32, pp. 465–466, Apr. 1984.

[17] M. E. Bialkowski, "Analysis of a coaxial-to-waveguide adaptor incorporating a dielectric coated probe," *IEEE Microwave Guided Wave Lett.*, vol. 1, pp. 211–214, Aug. 1991.

[18] R. L. Eisenhart, P. T. Greiling, L. K. Roberts, and R. Robertson, "A useful equivalence for a coaxial-waveguide junction," *IEEE Trans. Microwave Theory Tech.*, vol. MTT-26, pp. 172–174, Mar. 1978.

[19] J. M. Jarem, "A multifilament method-of-moments solution for the input impedance of a probe-excited semi-infinite waveguide," *IEEE Trans. Microwave Theory Tech.*, vol. MTT-35, pp. 14–19, Jan. 1987.

[20] J. J. Hug, "A probe-fed patch antenna array using a multi-layer parallel-plate dielectric waveguide feed network," M.S. thesis, Dept. Elect. Comput. Eng., Polytech. Univ., Brooklyn, NY, 1999.

[21] J. J. Hug and N. K. Das, "Multilayer feeding of microstrip sub-array using parallel-plate dielectric waveguides (PPDW)," in *IEEE AP-S Symp. Dig.*, vol. 3, July 2001, pp. 586–589.

[22] R. F. Harrington, *Time Harmonic Electromagnetic Fields*. New York: McGraw-Hill, 1984.

[23] N. K. Das and D. M. Pozar, "A generalized spectral-domain Green's function for multilayer dielectric substrates with applications to multilayer transmission lines," *IEEE Trans. Microwave Theory Tech.*, vol. MTT-35, pp. 326–335, Mar. 1987.

[24] ——, "A generalized CAD model for printed antennas and arrays with arbitrary multilayer geometries," in *Computer Physics Communication, Thematic Issue on Computational Electromagnetics*, L. Safai, Ed. Amsterdam, The Netherlands: North-Holland, 1991.

[25] N. K. Das, "Generalized multiport reciprocity analysis of surface-to-surface transitions between multiple printed transmission lines," *IEEE Trans. Microwave Theory Tech.*, vol. 41, pp. 1164–1167, July 1993.

[26] E. Krayszig, *Advanced Engineering Mathematics*. New York: Wiley, 1988.

Godfrey K. C. Kwan (S'97–M'99) was born in Hong Kong, in 1963. He received the B.Sc. degree (first-class honors) in electronic and communication engineering from the Polytechnic of North London, London, U.K., in 1986, the M.S.E.E. degree from the State University of New York at Stony Brook, in 1994, and the Ph.D. degree in electrical engineering from the Polytechnic University, Brooklyn, NY, in 1999.

In September 1994, he joined the Department of Electrical Engineering, Polytechnic University, Brooklyn. In 1983, he studied the French language at La Sorbonne, Paris, France. In 1984, he also studied at the l'Ecole Superieure d'Informatique-Electronique-Automatique, Paris, France. From 1987 to 1990, he was a Software Engineer with SITA Hong Kong and a Senior HLS Programmer with SITA New York from 1991 to 1994. From 1999 to 2000, he was a consultant for Sikorsky Aircraft, where he used finite-difference time-domain techniques in the analysis of antenna performance in helicopters. In July 2000, he joined Agilent Technologies, Rohnert Park, CA, as a Manufacturing Development Engineer in the Electrical Standards Laboratory. He is currently involved in the study of vector network analyzer calibration techniques and coaxial impedance standards used in 45 MHz–110 GHz frequency range. His research interests include computational electromagnetics, analytical and experimental study of dielectric waveguides and antennas, multilayer microwave integrated circuits, calibration standards, and techniques for vector network analyzers.

Nirod K. Das (S'87–M'88) was born in Orissa, India, on February 27, 1963. He received the B.Tech. degree in electronics and electrical communication engineering from the Indian Institute of Technology (IIT), Kharagpur, India, in 1985, and the M.S. and Ph.D. degree in electrical engineering from the University of Massachusetts at Amherst, in 1987 and 1989, respectively.

From 1985 to 1989, he was with the Department of Electrical and Computer Engineering, University of Massachusetts at Amherst, as a Graduate Research Assistant and then continued as a Post-Doctoral Research Associate during 1989–1990. In 1990, he joined the Department of Electrical Engineering, Polytechnic University of New York, where he has been an Associate Professor since 1997. He co-edited *Next Generation of MMIC Devices and Systems* (New York: Plenum, 1997). He also authored the computer-aided design (CAD)/instructional tool "PCAAMT," for microwave multilayer printed transmission lines and the simulation tool "UNIFY" for unified modeling of multilayer printed antennas and arrays. His research interests have been in the general areas of electromagnetics, antennas, and microwave and millimeter-wave integrated circuits. His recent research activities include numerical–analytical methods for electromagnetics, multilayered integrated circuits, leaky waves and applications, and artificial materials for microwave circuits and antennas.

Dr. Das is a member of the IEEE Antennas and Propagation Society (IEEE AP-S), the IEEE Microwave Theory and Techniques Society (IEEE MTT-S), and the New York Academy of Sciences. He currently serves on the Editorial Board of the IEEE TRANSACTIONS ON MICROWAVE THEORY AND TECHNIQUES, and the Technical Program Committee of the IEEE MTT-S International Symposia. He was the co-chair of the 1996 International Weber Research Institute (WRI) Symposium, Brooklyn, NY. He was the recipient of the 1990 Student Paper Award (Third Prize) presented by the US National Council of the International Scientific Radio Union (URSI) for his doctoral research work on multilayer printed antennas and the 1993 R. W. P King Paper Award (below 35 age group) presented by the IEEE AP-S.